Chapter 5

Cu-Cr and Cu-Fe Alloys Processed by New Severe Plastic Deformation: Microstructure and Properties

Kinga Rodak

Additional information is available at the end of the chapter

http://dx.doi.org/10.5772/intechopen.68954

Abstract

In this chapter, two techniques have been proposed for grain refinement in Cu-Cr and Cu-Fe alloys in different heat treatment conditions. First method, known as rolling with cyclic movement of rolls (RCMR), is appropriate for the manufacturing of ultrafine grained sheets and plates. The second method is called compression with oscillatory torsion (COT). Structural investigations of alloys were carried out, in particular, using a cold field emission gun/scanning electron microscope (FEG/SEM) equipped with an electron backscattering diffraction (EBSD) detector and a scanning transmission electron microscope (STEM). Quantitative studies of the microstructure based on the STEM images were performed using the "MET-ILO" software package. Mechanical properties were determined using an MST QTest/10 instrument equipped with digital image correlation (DIC). Based on the SEM and STEM observations, it has been shown that the alloys may exhibit a refinement of the ultra fine grained (UFG) structure in the 200–500 nm range with a mixture of low- and high-angle boundaries. Although the microstructure was refined significantly, the heterogeneity of the microstructure after the application of a high total effective strain is observed. Moreover, the low-angle boundaries formed at the early stages do not continuously transform into high-angle boundaries.

Keywords: SPD, mechanical properties, microstructure, STEM, EBSD

1. Introduction

Severe plastic deformation (SPD) is a metal forming process used to introduce ultra-high plastic strains into a bulk metal in order to refine the grain structure of metallic materials to the submicrometer (100–1000 nm) or even nanometer (less than 100 nm) range. A finer grain size increases the hardness, the yield stress, and the fracture toughness of the material [1–9]. Overall, SPD deformation is recognized as a potential tool for superplastic deformation at

lower temperatures and high strain rates [2–5]. While in the conventional metal forming processes, the imposed plastic strain is generally low, SPD imposes an extremely large strain on the bulk metal without changing the shape of the metal necessary for chosen techniques [2, 3]. Practically, obtaining a large plastic deformation is difficult because in most metal-forming processes the deformation is limited by the failure of either the material or the tool. Considering the deformation processing conditions, the heterogeneity in microstructure formation was often observed across the bulk specimen depending on the introduced strain [3, 6, 7]. From the literature it is known [5–7] that very fine and highly disoriented grain structures obtained in different bulk metals and alloys are created as a result of short- and long-range intersecting shear bands produced by plastic deformation. Additionally, the local dynamic recovery and recrystallization processes [5, 7] also contribute to the grain refinement. Distinct structures are either dislocation-free or with dislocations and fine grains that are highly or weakly disoriented and are obtained during the SPD deformation. The evolution and characterization of the new grain/subgrain boundaries appear to be very important for their influence on the mechanical and functional properties of SPD materials. Additionally, the SPD problem is connected with the effect of the strain path on the structure formation, i.e. a broad variety of structures that show differences in the grain size, shape, and crystallographic texture [7–9].

The influence of SPD on the microstructure refinement is more complicated when the precipitation strengthening mechanism of alloys is taken into account. The effect of the secondary phase particles on the grain refinement mechanisms during severe deformation processing is still topical and has been explored extensively [10–14]. The presence of second phase particles is a source of a significant strengthening resulting from the interaction of dislocations. The strength of this interaction depends on the chemical composition, size, distribution, and the degree of coherence with the matrix. In engineering alloys, the second phase particles may take the form of dispersoids, fine precipitates, and large primary particles that may show quite different effects on the grain refinement during SPD processing.

Two original methods patented at Silesian University of Technology, Faculty of Materials Engineering and Metallurgy in Poland for grain refinement are discussed in this paper: the first method is called rolling with cyclic movement of rolls (RCMR) and is appropriate for the manufacturing of ultrafine grained sheets and plates. The second method allows large deformations and is called compression with oscillatory torsion (COT). This process combines two deformation methods: (1) the compression process which is effective for obtaining high mechanical properties and a microstructure composed of elongated grains with a high dislocation density; (2) the torsion process which is effective for obtaining a higher plasticity and a microstructure consisting of quite equiaxed subgrains with a small dislocation density inside the subgrains. The combination of these methods in a single deformation procedure enables the optimization of the microstructure and mechanical properties. COT investigations were performed for Cu and Al [14–19] and this method was recognized as an effective tool for obtaining ultrafine grains/subgrains with a mixture of low- and high-angle grain boundaries.

In this chapter, we demonstrate the effectiveness of COT and RCMR deformation as a technique for studying large strain deformation in Cu-Fe and Cu-Cr alloys at room temperature.

Cu-Cr alloys are used in numerous applications where a combination of excellent mechanical strength and electrical conductivity is required [20–23]. They can be important materials for railway contact wires and electrodes for spot welding. Meanwhile, Cu-Fe alloys are commonly used as electrical device components such as semiconductor lead frames and electrical connectors [24].

The Cu-Cr and Cu-Fe alloys belong to the class of precipitation-hardened alloys, and therefore, the problem of the initial structure (after solution and aging treatment at different parameters) is discussed in this paper. The aim of the present research is also extended to the evaluation of whether it is possible to obtain smaller grain sizes and, consequently, to improve the mechanical properties of the material if the processed materials have different initial structures (different states of heat treatment). The obtained results may be useful for constructing a complete picture of the structure and properties evolution in these alloys during RCMR and COT processing.

It should be noted that Cu-Cr and Cu-Fe alloys were chosen for the present study because these alloys are readily produced by SPD techniques at room temperature. This is because these alloys belong to the class of face-centered cubic precipitation hardenable alloys that are much more thermally and mechanically stable during the deformation than the pure Cu without the structural instabilities such as grain coarsening.

2. Refinement structure of Cu-Cr and Cu-Fe alloys by SPD techniques

Annealed high-purity of Cu exhibits a low strength of nearly 100–200 MPa and attractive physical properties such as its high electrical conductivity. The extensive dynamic recovery balancing the multiplications and annihilation of the dislocations is the limiting factor for the grain refinement in Cu [15, 16].

The introduction of solute atoms in the Cu matrix is the first route for the strengthening of conventional Cu alloys. The introduction of solute atoms into a solid solution produces an alloy that is stronger than the pure Cu due to the differences in the radius, modulus, and valence between the Cu matrix and solute atoms [20–24]. On the other hand, the alloying process results in the degradation of electrical conductivity. Moreover, after the deformation (SPD), the strength evidently increases but the conductivity decreases slightly due to the introduction of a large quantity of dislocations by cold deformation. The selection of the optimum properties for electrical applications always involves a trade-off between the mechanical and electrical properties. The precipitation effect during age hardening in Cu alloys gives rise to a subsequent effect improving the strength and also the electrical properties. The presence of precipitations reduces the dislocation mobility and the rate of dynamic recovery in alloys. In this case, the dislocations in the deformed Cu cannot be easily annihilated, very often leading to nonequilibrium dislocation clustering near the boundaries.

Little data is available in the literature for the Cu-Cr and Cu-Fe alloys after the application of SPD. The available data for the influence of SPD on the structure and mechanical properties

are presented and summarized in **Table 1**. Examination of the data clearly shows that SPD processing was applied for the alloy after casting or quenching. It should be noted that an application of SPD deformation for the refinement of the structure of these alloys can produce grain sizes in the 100–400 nm range.

Material/SPD process	Initial state	Microstructure	Mechanical properties	References
Cu-0.5Cr/ECAP route A, $\varepsilon = 6.4$	Solid solution at 1000°C/0.5 h	Pancake shaped grains with high-angle boundaries with thickness of 100 nm. Many boundaries are curved, indicating the presence of high internal stress	UTS= 484 MPa Electrical cond. 35% of IACS HV0.3 = 145	[23]
Cu-0.36Cr ECAP route A,	Solid solution at 1025°C/40 min	Pancake-fragmented structure with lamellar boundaries. Grain diameter of 0.41 μm. Fraction of HABs0.75	HV0.2 = 150	[21]
Cu-0.75Cr, HPT, $\varepsilon = 4.8$	Solid solution at 1025°C/2 h	Average grain size-209 nm, dislocation density $\rho = 38 \times 10^{14}$ m^{-2}	HV (MPa) = 1740 after HPT Electrical cond. 34% of IACS	[20]
Cu-0.5Cr-0.1Ag HPT, 6 GPa, 10 rev.	Solid solution at 1025°C/1 h	Homogeneous structure UFG with the mean grain size of about 200 nm	UTS = 840 MPa, $A = 10\%$	[22]
Cu-Fe_P ECAP route Bc route A	As-cast alloy	Ultrafine grain structure with most dislocations found on the grain boundaries and the interior of the grain showing a lower dislocation density. The grains are not far from equiaxed, ranging from 50 to larger than 200 nm	HV = 166	[24]

Table 1. Effect of SPD deformation on grain size refinement in Cu alloys.

3. Materials and experiment

Copper alloys with addition of 0.6 wt% Cr (C18200) and 2 wt% Fe (C19400) were produced using induction melting of highly pure components. **Figure 1** shows the microstructure of the samples after casting with columnar grains. Inside the grains of CuCr0.6 alloy, for example, the Cu, Cr, and P elements are homogeneously distributed in the alloy after the casting (**Figure 2**). The ingots with the diameter of 50 mm were hot-deformed on the rods. Subsequently, the rolled bars underwent different heat treatments such as the solution treatment at 1000°C for 3 h (P state), followed by quenching into iced water and aging at 500°C for 2 h (S1 state), and 700°C for 24 h (S2 state).The microstructures of the CuCr0.6 and CuFe2 alloys after the solution treatment are characterized by the presence of equiaxed grains with heterogeneously distributed undissolved large Fe and Cr precipitates [14, 22, 23]. The aging treatment at 500°C for 2 h results in the formation of homogeneously distributed coherent precipitates within the matrix. As the aging temperature and time are increased, the precipitates lost coherence with

http://dx.doi.org/10.5772/intechopen.68954

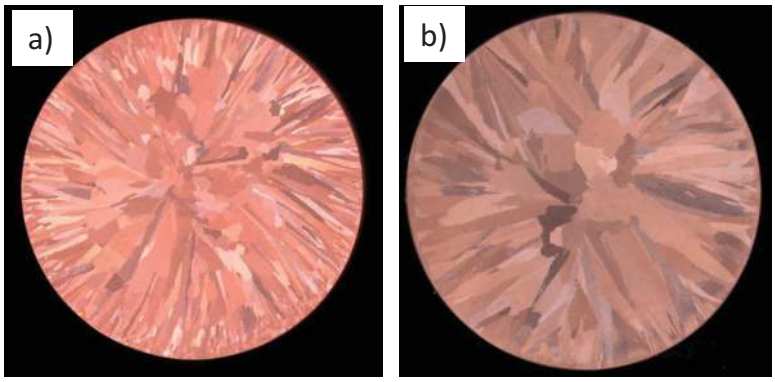

Figure 1. Microstructure of CuFe2 (a) and CuCr0.6 (b) samples after casting.

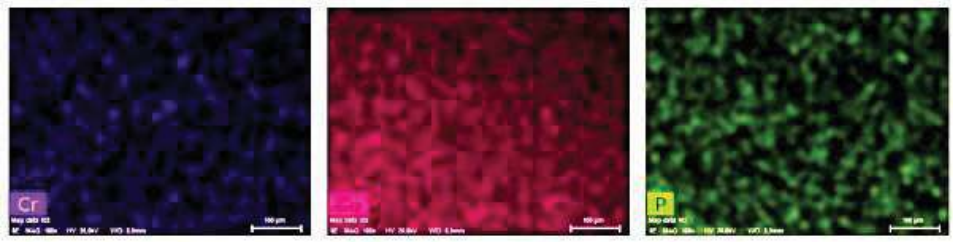

Figure 2. Distribution of Cu, Cr, and Pin the CuCr0.6 alloy after casting.

the matrix and the number of the particles within the matrix decreased (the spacing between the particles increased). The measured microstructural parameters of the precipitates are presented in **Table 2**. The samples were mechanically machined for appropriate dimensions for RCMR and COT deformation.

Scanning electron microscopy (FEG SEM INSPECT F by FEI equipped with an electron backscattering diffraction (EBSD) detector) was used to characterize the microstructures of the deformed alloys. Additionally, a scanning transmission electron microscope (STEM) Hitachi HD-2300A operated at 200 kV was applied for substructure characterization. The quantitative

State of material	CuCr0.6		CuFe2	
	d	*λ*	*d*	*λ*
P	0.7 μm	2.5 μm	0.5 μm	4.5 μm
S1	20 nm	60 nm	20 nm	40 nm
S2	270 nm	520 nm	100 nm	200 nm

Table 2. Measured microstructural parameters: *d*: average particle diameter, *λ*: average distance between the particles in CuCr0.6 and CuFe2 alloys after heat treatment.

studies of the structure parameters (for example: grain/subgrain and precipitate sizes) based on the STEM images were performed using the "MET-ILO" software package.

The mechanical properties were determined using an MST QTest/10 instrument equipped with digital image correlation (DIC). The use of the DIC method is advantageous due to its non-contact character and ability to perform high precision strain measurements. A SIGMATEST electric conductivity instrument was used to measure the conductivity. Due to the heterogeneity of the plastic deformation in the sample after the COT deformation, structural studies and mechanical investigations were performed on the samples extracted at the distance of 0.8 of the radius in the longitudinal plane section. The heterogeneity of the plastic deformation in the RCMR method causes a considerable differentiation of the structure. Microstructural observations (SEM) and evaluation of the mechanical properties were performed in the transverse plane section located at the height of ~0.8 of the specimen height. Since STEM analysis was not possible on the transverse section due to the small dimensions of the sample, STEM observations of the thin foils parallel to the rolling plane were performed at the distance of 0.6 of the specimen height.

Vickers hardness (HV0.2) measurements were carried out using a FM-310 Future-Tech hardness machine with the load of 200 g for 15 s. Microhardness measurements were performed in a plane parallel to the compression direction. To accurately describe the heterogeneity occurring during the COT processing, hardness maps were obtained for the longitudinal sections of the samples. The distance between the measuring points was about 0.5 mm, giving approximately 200 measurement points used to create the hardness maps.

The mechanical properties were determined using an MST QTest/10 machine equipped with digital image correlation (DIC). The tensile tests were performed at room temperature at the initial strain rate of 1×10^{-3} s^{-1}. Small tensile specimens with the total length and thickness of 8.6 and 0.3 mm, respectively, were used to measure the mechanical properties.

4. Production of ultrafine grained structure of CuCr0.6 and CuFe2 alloys by RCMR method

Several excellent techniques have been developed for creating tapes and strips products including the methods of constrained groove pressing (CGP) and accumulative roll-bonding (ARB). According to the reports in the literature [2], the CGP and ARB techniques exhibit several advantages over other SPD processes because (1) they do not require forming facilities with a large load capacity and expensive dies; (2) the amount of the material that can be produced is not limited. These methods are appropriate for the manufacturing of nanocrystalline and ultrafine grained sheets and plates. Rolling with cyclic movement of rolls method (RCMR) is a severe plastic deformation process that allows large deformations and is based on the rolling connected with the movement of the material layers in a direction perpendicular to the main direction of the rolling. By repeating this procedure, very high strains have been introduced into the material and a significant structure refining effect is obtained. This original method of deformation has been patented by Silesian University of Technology,

Faculty of Materials Engineering and Metallurgy in Poland. Compared to the various other SPD methods, the RCMR method exhibits the following advantages: the method is simple and can be carried out using conventional testing machines. It is possible to obtain a wide range of strain rates and high total effective strain values. RCMR can be applied to large-scale workplaces and thus has the potential for application in industry.

Figure 3 shows the RCMR setup. The rolling mill consists of two working rolls, the power unit, and the mechanism for the cyclic movement of the rolls transverse to the rolling direction. (The rolling mill without the mechanism for the cyclic movements of rolls is a typical example of setup for conventional cold-rolling.) During RCMR processing, the rolls rotate around an axis and, in addition, axial movements of the rolls in opposite directions are realized.

The structure and mechanical properties are found to depend strongly on the imposed total effective strain ε_{ft} given by Eqs. (1)–(3):

$$\varepsilon_{ft} = \sum_{i=1}^{n} \sqrt{\varepsilon_{hi}^2 + \varepsilon_{ti}^2}, \tag{1}$$

$$\varepsilon_{hi} = /\ln \frac{h_i}{h_{i-1}}/, \tag{2}$$

$$\varepsilon_{ti} = \frac{4 \cdot f \cdot A \cdot \sqrt{(h_i - h_{i-1}) \cdot \frac{D}{2}}}{\sqrt{3} \cdot v \cdot (h_{i-1} + h_i)} \tag{3}$$

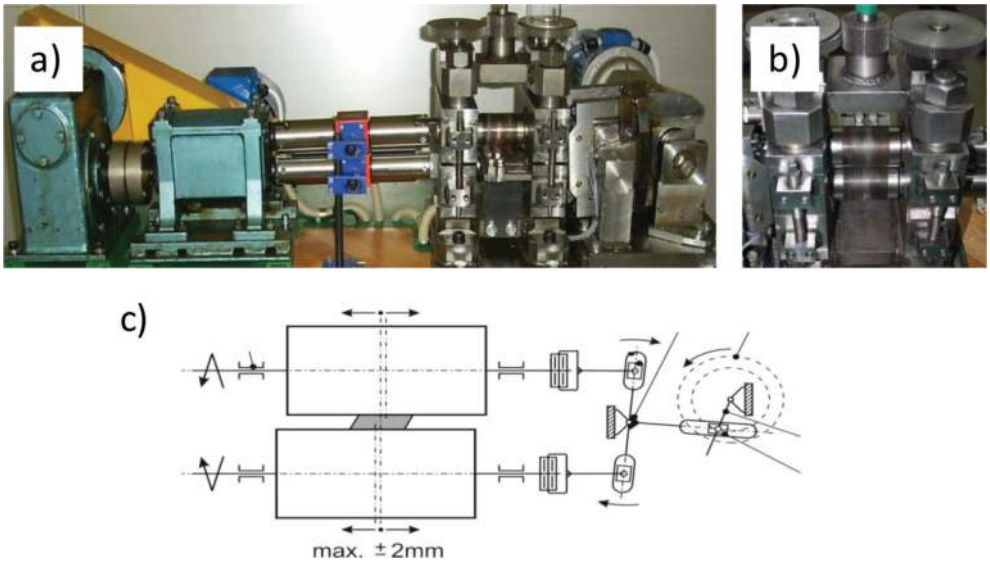

Figure 3. (a) RCMR setup; (b) working rolls; and (c) RCMR scheme.

Here, εft is the total effective strain, εhi is the strain contributed by the rolling reduction, εti is the strain included by the transverse movement of the working rolls, n is the number of passes, hi−1, hi are the heights of the sample before and after the unit pass (reduction), and A is the amplitude of the cyclic roll movement, v – (%), rolling rate , f – frequency of the transverse roll movement, D- diameter of rolls – here D=100mm

The deformation path can be controlled by changing the proportions of the following parameters: the rolling reduction ε_h (%), rolling rate v (rpm), amplitude of the transverse roll movement A (mm), and frequency of the transverse roll movement f (Hz).

The changes in the rolling forces and torques with the number of passes for the CuCr0.6 alloy are presented in **Figure 4**.

For all passes, the values of the rolling forces and rolling torques are larger for the conventional rolling than for RCMR. Examination of the obtained data shows that the additional transverse deformation during RCMR has a significant effect, decreasing the processing parameters. The data for the height of the samples after the deformation (1–6 passes) for rolling and RCMR process are

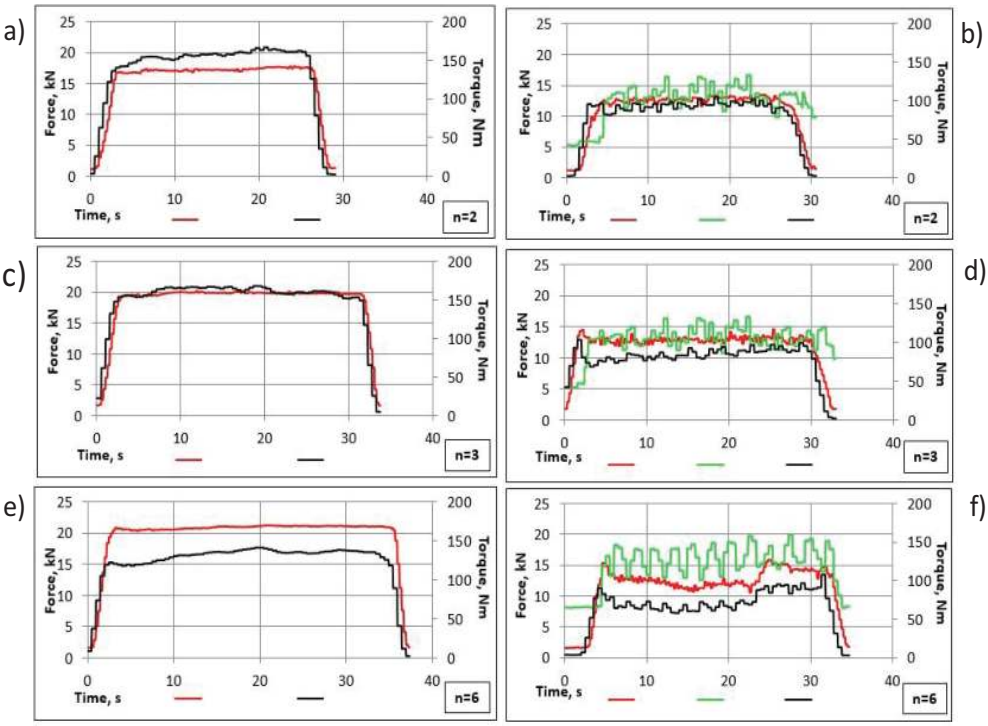

Figure 4. Changes in rolling forces and torques with the number of passes for CuCr0.6 alloy sample (S2 state), (a), (c), (e) conventional rolling, (b), (d), (f) RCMR. Parameters: rolling rate v = 1 (rpm), amplitude of the transverse roll movement A = 0.8 (mm), and frequency of the transverse roll movement f = 1.5 (Hz). Legend: red line-rolling force, black line-torque, green line-axial force.

http://dx.doi.org/10.5772/intechopen.68954

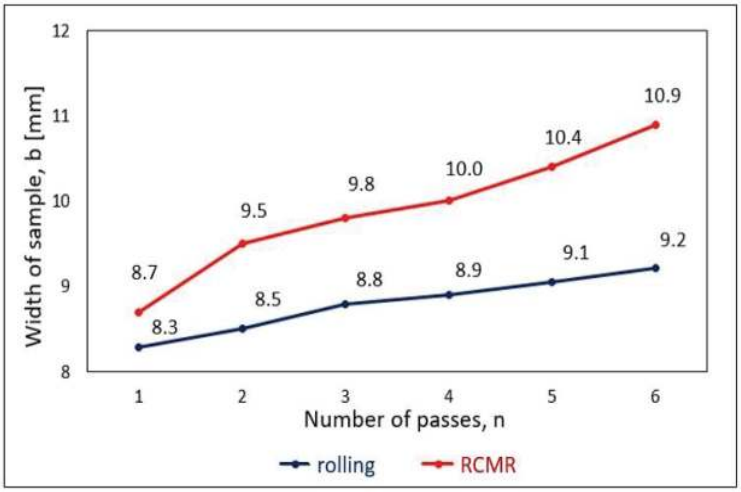

Figure 5. Changes of sample width of CuFe2 (P state) for rolling and RCMR as a function of the number of passes. Parameters: rolling rate v = 0.7 (rpm), amplitude of the transverse roll movement A = 0.8 (mm), and frequency of the transverse roll movement f = 1.5 (Hz).

presented in **Figure 5**. These results show that larger heights are obtained for the rolling samples than for the RCMR samples. However, the obtained values are very close to each other.

The changes in the total effective strain as a function of the number of passes during rolling and RCMR of the CuCr0.6 alloy at selected parameters are presented in **Figure 6** while **Figure 7** presents the obtained results for the dependence of the total effective strain of the CuFe2 alloy on the rolling rate. The obtained results show that the rate of the RCMR has a significant impact on the value of the total effective strain. Generally, examination of the obtained results shows that for the RCMR process, the total effective strain values in each pass are different and for RCMR, the values are 3–5 times higher than those obtained for conventional rolling. This means that the calculated total effective strain values in the RCMR process are not constant during subsequent passes. This is due to the heterogeneity in the deformation in a volume of the rolled strip and the phenomena occurring at the contact surfaces between the working rolls and strips. The obtained results show evidently that in the conventional metal forming process such as cold rolling, the imposed plastic strain is generally less than about 2.0 (**Figure 6**). In the RCMR process an extremely large strain is possible to impose without additional changes in shape (**Figures 5** and **6**).

The sample temperature during conventional deformation and RCMR was investigated using a thermal imaging camera (**Figure 8a** and **b**). The temperature rise was calculated as the difference between the maximum of the surface temperature of the rolled sample and the ambient temperature (adopted as 24°C) (**Figure 8c**). It is evident that for the RCMR samples, the temperature rise is higher than that for the conventional sample. Increase of the temperature during RCMR is due to the additional work done by the plastic deformation resulting from the transverse roll movement. The temperature increase during the deformation can cause a reduction of the rolling force and rolling torque during the RCMR deformation.

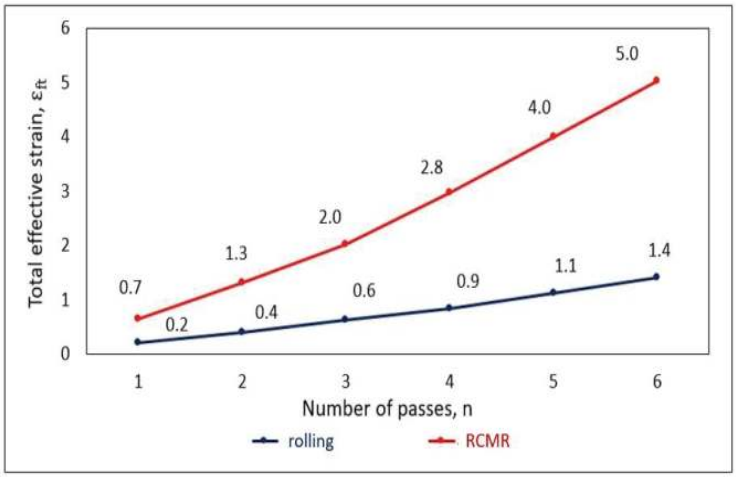

Figure 6. Changes of total effective strain in CuCr0.6 alloy (S2 state) for rolling and RCMR with number of passes. Parameters: rolling rate v = 1 (rpm), amplitude of the transverse roll movement A = 0.8 (mm), and frequency of the transverse roll movement f = 1.5 (Hz).

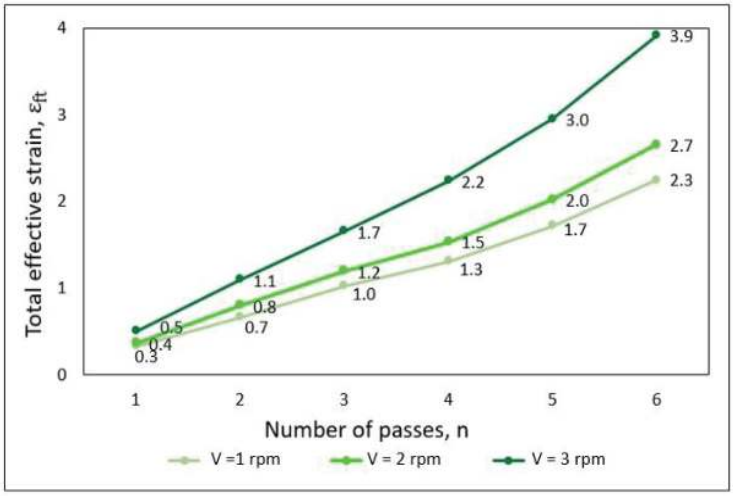

Figure 7. Changes of total effective strain in CuFe2 alloy (P state) for RCMR with number of passes and rolling rate. Parameters: amplitude of the transverse roll movement A = 0.8 (mm), and frequency of the transverse roll movement f = 1 (Hz).

The examples of the samples after RCMR processing for the rolling rates of 1, 2, and 3 rpm are presented in **Figure 9** that also shows a characteristic surface that depends on the applied parameters and could indicate the heterogeneity in the plastic deformation.

http://dx.doi.org/10.5772/intechopen.68954

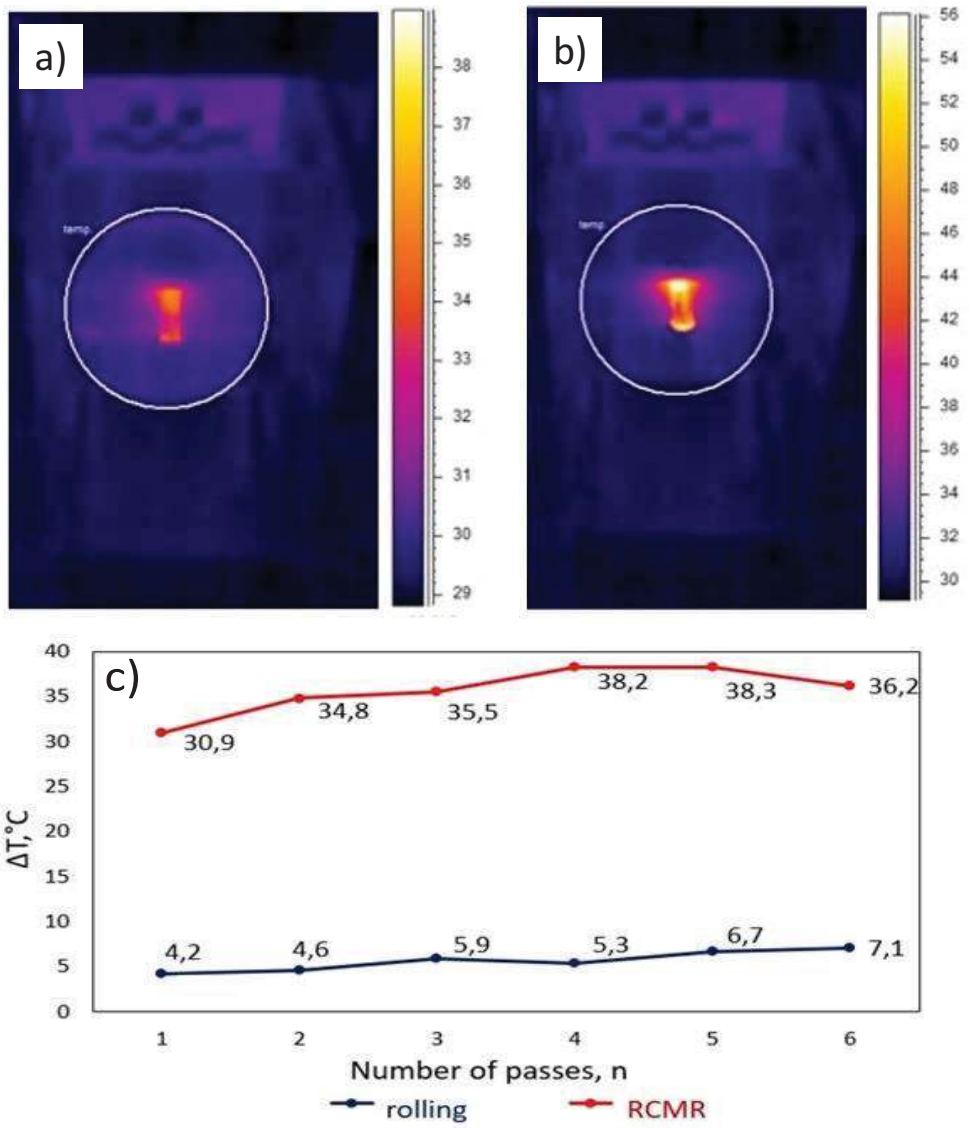

Figure 8. Thermographical images of CuFe2 (S1 state) sample surfaces after four passes obtained for: (a) rolling sample, (b) RCMR sample, and (c) changes in the temperature rise for rolling and RCMR with the number of passes. Parameters: rolling rate v = 1 (rpm), amplitude of the transverse roll movement A = 0.8 (mm), and frequency of the transverse roll movement f = 1 (Hz).

The transverse section of the RCMR-processed samples (**Figure 10**) exhibits inhomogeneous features along the through-thickness direction. It is clearly observed that unlike the middle, top, and bottom regions, the side region of the samples exhibits a near nondeformable structure.

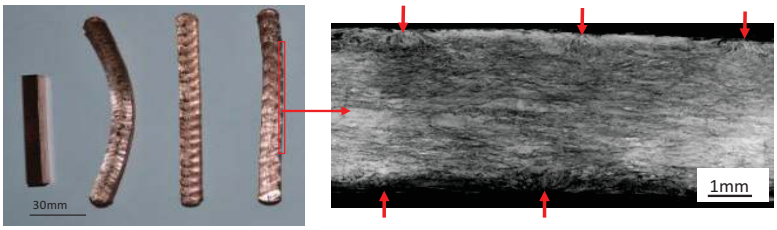

Figure 9. Macrostructure of RCMR samples before deformation and after RCMR with rolling rates of 1, 2, and 3 rpm. Characteristic "serrations" on the contact surfaces of the rollers as a result of transverse movement of rolls. Visible effects of RCMR on the lateral surface of the sample are marked by arrows.

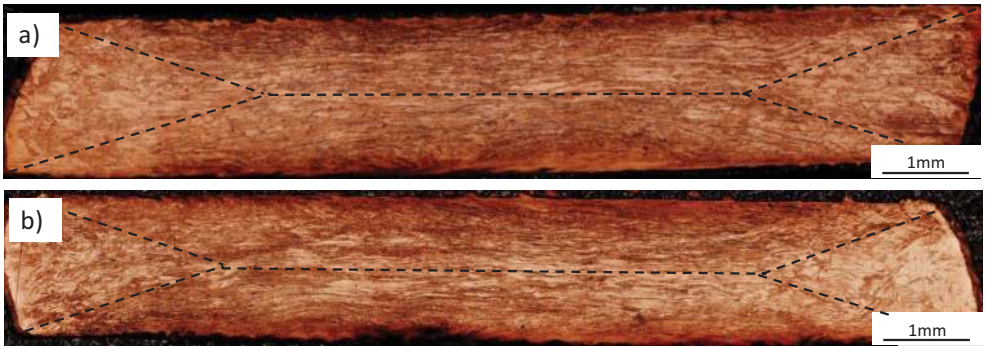

Figure 10. Transverse section of CuFe2 samples after RCMR for (a) S1 and (b) S2 states. Parameters: rolling rate $v = 1$ (rpm), amplitude of the transverse roll movement $A = 0.8$ (mm), and frequency of the transverse roll movement $f = 1.5$ (Hz), number of passes = 6.

The image in **Figure 10** also shows that the overall shape of the sample is asymmetric. This is attributed to a minor misalignment of the rolls during processing. The region of the deformed sample maintains the orientation of the as-received material (the side area), suggesting a low deformation magnitude while a different orientation of the structural features is observed in another area, suggesting a high deformation magnitude.

The heterogeneous features observed along the thickness of the samples are attributed to a difference in the deformation magnitude and can be easily seen at higher magnification (**Figure 11**).

STEM investigations confirm the heterogeneity in the refinement structure (**Figure 12**) with the microstructural observations revealing the coexistence of alternating elongated grains with a high dislocation density (**Figure 12b**)and the fine equiaxed grain without internal dislocations (**Figure 12a**).

Figure 13 shows a color-coded distribution of the hardness along the half-transverse sections of the CuFe2 alloy sample after RCMR for selected numbers of passes. It is observed that significant hardness variations are presented in the sample, with higher hardness values observed in the top and bottom areas of the sample where transverse rolling was imposed and

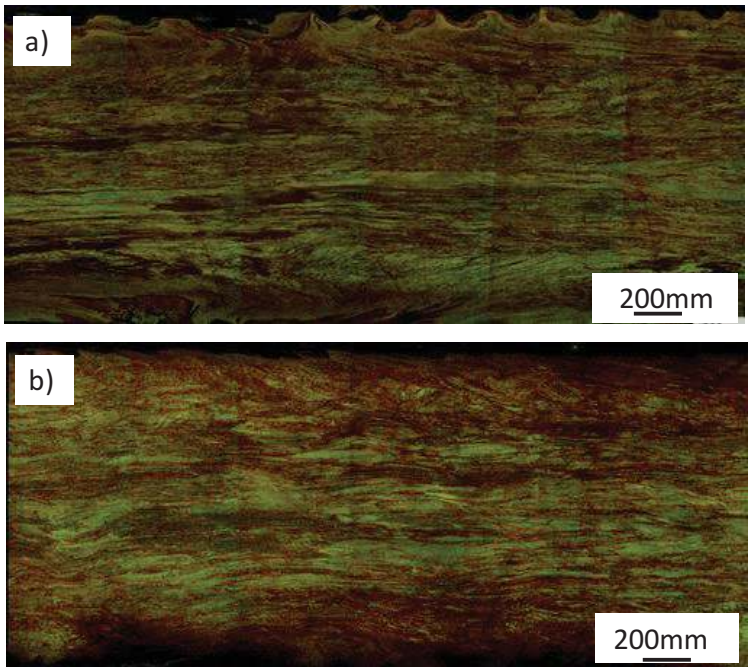

Figure 11. Transverse section of (a) CuCr0.6 sample (P state) after RCMR with parameters: rolling rate v = 0.7 (rpm), amplitude of the transverse roll movement A = 0.8 (mm), and frequency of the transverse roll movement f = 1.5 (Hz), number of passes = 6, (b) CuFe2 sample (S2 state) after RCMR with parameters: rolling rate v = 1 (rpm), amplitude of the transverse roll movement A = 0.8 (mm), and frequency of the transverse roll movement f = 1.5 (Hz), number of passes = 6.

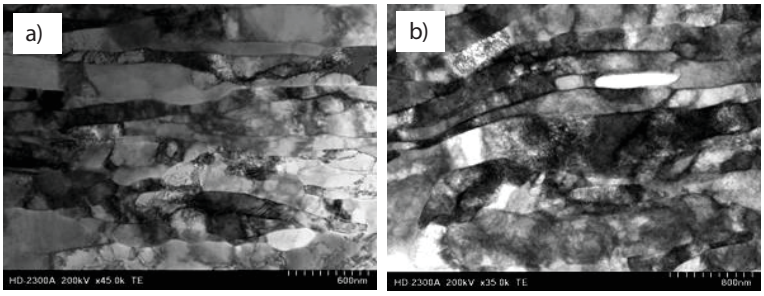

Figure 12. STEM microstructures of CuFe2 (S2 state) sample taken from different areas after RCMR with parameters: with parameters: rolling rate v = 1 (rpm), amplitude of the transverse roll movement A = 0.8 (mm), and frequency of the transverse roll movement f = 1.5 (Hz), number of passes = 6.

lower hardness values are observed in the central areas. It is important to note that the hardness distribution in the samples is in agreement with the microstructures shown in **Figures 10** and **11**.

The measured mechanical parameters for CuFe2 and CuCr0.6 alloys are presented in **Table 3** and it can be seen that solid solution treated CuFe2 and CuCr0.6 alloys that exhibit strain hardening, low strength, and high ductility. The best strength properties were obtained for the alloy in the S1 + RCMR state while the strength properties obtained for the alloys in the P + RCMR and S2 + RCMR states were comparable. The samples after the deformation show elongation to fracture (A_c) values in the 4–7% range and a uniform elongation (A_{gt}) of ~1%. These results are in accordance with the STEM observations of the microstructure and confirm that only fine coherent precipitates are active for the blocking of the dislocations. The lack of coherent precipitates in the P + RCMR and S2 + RCMR states effectively decreases the dislocation generation rate with the large particles.

In general, it should be noted that the SPD-processed materials generally have very high strength and hardness compared with conventional deformed materials. RCMR method belongs to cyclic method of deformation and from this point of view the tensile strength of materials with ultrafine grains does not become much higher compared with conventional process. Evidently, it is observed that tendency of ductility increases in materials deformed by RCMR process. This is the effect of structure formation. It is known that the plastic deformation results in microstructural refinement through formation of a three-dimensional dislocation boundary structure. The dislocation boundaries formed during conventional rolling are predominantly rotation boundaries, so that the refinement is not just spatial, but

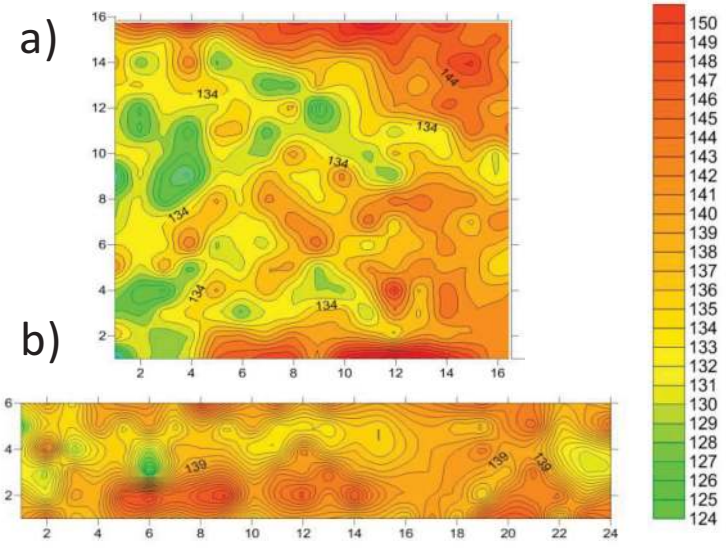

Figure 13. Distribution of measured hardness values on the transverse section of samples CuFe2 (P state) for two passes (a); and six passes (b). Parameters: rolling rate v = 1 (rpm), amplitude of the transverse roll movement A = 0.8 (mm), and frequency of the transverse roll movement f = 1.5 (Hz).

Material state		YS (MPa)	UTS (MPa)	A_{gt} (%)	A_c (%)	HV	IACS (%)
CuCr0.6	Initial state	97 ± 4	214 ± 5	22.5 ± 1	26.0 ± 1	43 ± 4	40
	Quenching + RCMR	363 ± 5	393 ± 9	1 ± 0.2	4.7 ± 0.5	123 ± 15	43
	Aging at 500°C/2 h + RCMR	513 ± 7	539 ± 7	1.1 ± 0.1	4.8 ± 0.6	180 ± 6.5	83
	Aging at 700°C/24 h + RCMR	324 ± 9	360 ± 5	1.2 ± 0.2	4.4 ± 0.2	132 ± 9	86
CuFe2	Initial state	148 ± 5	246 ± 4	14.2 ± 0.5	17.7 ± 0.6	60 ± 4	28
	Quenching + RCMR	356 ± 7	361 ± 6	1.0 ± 0.5	4.7 ± 0.5	126 ± 14	22
	Aging at 500°C/2 h + RCMR	388 ± 7	393 ± 6	0.9 ± 0.3	4.0 ± 0.3	150 ± 16	41
	aging at 700°C/24h+RCMR	366 ± 7	371 ± 5	1.2 ± 0.3	7.0 ± 0.3	133 ± 9	34

Table 3. Measured mechanical parameters: yield strength (YS), ultimate tensile strength (UTS), uniform elongation (A_{gt}), and elongation to fracture (A_c) of deformed CuCr0.6 and CuFe2 alloys.

also crystallographic. During RCMR deformation dislocation mobility is increased as a result of temperature increase, for example, thereby enabling the establishment of a fully three-dimensional boundary structure. The materials having such a structure are characterized by a number of specific properties including significantly higher yield point or ductility than that produced by conventional deformation methods as rolling.

The microstructure formation and the influence of the microstructure on the mechanical properties in CuFe2 alloy during the RCMR deformation have been well-documented elsewhere by the author [14]. In these studies, it has been clearly demonstrated that the grain refinement process observed on the cross-section plane is not homogeneous for all deformation states and that the impact of transverse rolling on the material is most apparent for the surface layers. It is found that the samples in all states (P, S1, S2) mostly exhibit lamellar/elongated structures with a mixture of low- and high-angle boundaries. It was also clearly shown that the deformation introduced into the material during RCMR does not guarantee the development of a refined microstructure with a high fraction of ultrafine grains with high-angle boundaries. The heterogeneity character depends on the structure in the initial state (heat treatment conditions) as schematically shown in **Figure 14**. The differences in the grain refinement can be understood by considering the intensity of the RCMR deformation of the sample in the cross section. For the S1 sample, the microstructural refinement is less pronounced in the volume of the sample, because coherent particles strongly affect the grain/subgrain size refinement. The lack of efficient barriers in the form of a high amount of dislocations leads to the comparable intensities of RCMR deformation for the cross sections of the P and S2 samples.

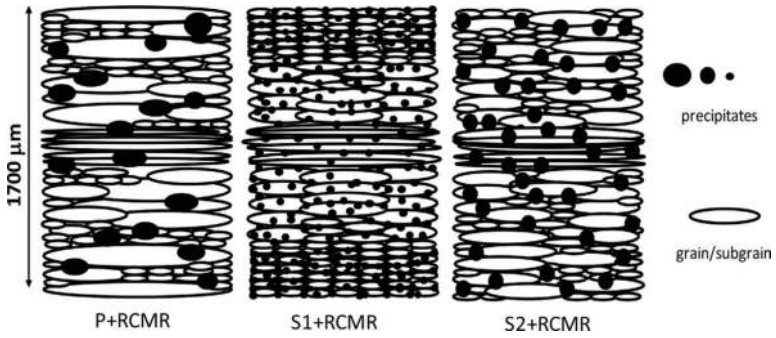

Figure 14. Scheme of microstructure refinement in RCMR processed samples.

5. Production of ultrafine grained structure of CuCr0.6 and CuFe2 alloys by COT method

Compression with oscillatory torsion (COT) is the second method patented by Silesian University of Technology, Faculty of Materials Engineering and Metallurgy in Poland and discussed in this paper. This processing technique can obtain a sub-micrometer grain size in a short time of deformation. **Figure 15a** and **b** present, respectively, a schematic of the COT setup as well as the illustration of the deformation of the samples by the simultaneous application of compression and oscillatory torsion which is the basic principle of the COT method. The method is characterized by the heterogeneity of deformation with the most intense deformations occurring at locations that are closest to the lateral surfaces of the material resulting from the application of the torsional moment. The oscillating course of the flow stress σ_p in the range σ_{pmin}–σ_{pmax} is caused by the cyclical variation of the torque M_t from 0 to M_{tmax} (**Figure 15c**).

These SPD techniques were adopted for grain size refinement in Cu and Al [15, 17].

Due to the complexity of the deformation process, the effective strains were calculated following the Huber-Mises-Hencky method and are given by

$$\varepsilon_f = \sqrt{\varepsilon^2 + \frac{\gamma^2}{3}}, \tag{4}$$

where ε is the deformation induced by the uniaxial strain and γ is the shearing strain.

The total effective strain ε_{ft} is expressed as the sum of effective strains obtained from Eq. (4) in a single phase of deformation as:

$$\varepsilon_{ft} = \sum_{n=1}^{n} \varepsilon_{fn}, \tag{5}$$

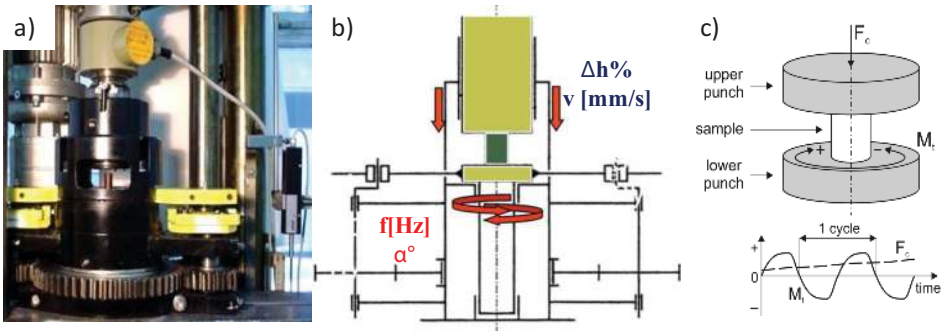

Figure 15. (a) Setup of COT, (b) schematic illustration of COT, and (c) scheme of the sample.

where n is the number of the deformation phases. The single phase comprises a torsion of the sample in one direction with a simultaneous decrease of the height.

The value of the total effective strain ε_{ft} can be controlled by changing the proportions of the following parameters: torsion frequency f in the range of 0–1.8 (Hz), compression rate v maximal 0.66 (mm/s), torsion angle α in the range of 0 to ±8 (°), and true reduction Δh (mm). **Table 4** shows the dependence of the changes in the compression force on the initial state of alloys for COT deformation. For all samples, the values of the compression force are larger for S1 state.

To illustrate the heterogeneity in the mechanical properties resulting from the COT deformation for the samples with different initial states (heat treatment), hardness distribution maps were created for selected samples. **Figures 16** and **17** show a color-coded hardness distribution along the half-longitudinal sections of the CuCr0.6 alloy sample prior to the deformation and after COT processing at ε_{ft} = 38, respectively. It is observed that the hardness variation depends on the distance from the center (**Figure 17c–e**). Higher hardness levels are observed around the 0–0.5r areas where influence of the compression process can be seen clearly. Lower hardness magnitudes are observed near the 0.5–1r distance from the center.

The higher hardness at a moderate distance from the center is typical for elongated structures with a high dislocation density. This region is quite different from the region near the surface with the refined equiaxed grains/subgrains. With the increase of the deformation ε_{ft} = 61, the homogenization of the hardness variation is not observed (**Figure 18**). Examination of the hardness distribution shows that local microareas with smaller hardness values are present in the processed samples. Therefore, the samples produced with COT exhibit heterogeneous hardness along the thickness of the samples. The increased deformation value has a moderate influence on the hardness distribution along the thickness of the sample. The increase of the deformation from ε_{ft} = 38 to 61 is not very effective for increasing the hardness. The Vickers hardness corresponds rather well to the microstructure evolution and the obtained results suggest that the Vickers hardness is affected by the dislocation structure rather than by the grain/subgrain sizes and boundaries misorientations. A coarse structure with a highly developed dislocation density gives hardness values that are larger than those for a well-defined fine-grained structure with a lower dislocation density.

Heat treatment	CuFe2		CuCr0.6	
	ε_f = 38	ε_f = 61	ε_f = 38	ε_f = 61
	Compression force *F* [kN]			
P + COT	22.7	58.0	14.3	46.9
S1 + COT	33.0	60.5	39.7	61.4
S2 + COT	24.8	58.0	25.0	58.3

Table 4. Dependence of the changes in the compression force on the initial state of alloys.

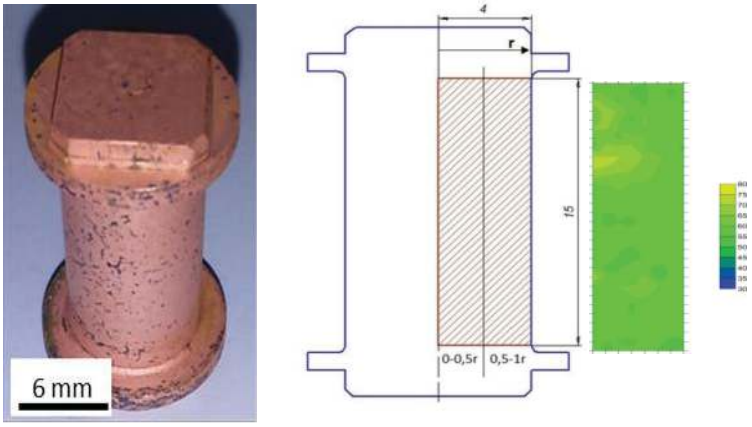

Figure 16. Distribution of measured hardness values on the longitudinal section of CuCr0.6 sample in initial (P) state before deformation.

Figure 19 shows the example of EBSD maps of the CuCr0.6 samples deformed at ε_{ft} = 45. Even though the original grains were plastically deformed, the grains are not significantly elongated perpendicular to the compression direction. This means that the compression does not have a strong effect on the deformed microstructure. The original grain boundaries are very jagged (the grains are comprised of a partially bulged original grain boundary) and the deformed grains are delineated by irregular bands due to the deformation occurring on different slip systems. Intersections of the deformation bands give rise to elongated grains/subgrains with mostly low-angle boundaries with misorientation angles largely in the 2–5° range, indicating a high density of cell and subgrain structures (**Figure 19a** and **b**).

In other areas, the refinement microstructure became better organized and the new boundaries were characterized by misorientation angles in the 5–15° range (**Figure 20a**). These microstructures involve the annihilation and rearrangement of the dislocations and were characterized for the P and S2 states (**Figures 19a**, **b**, **e**, **f**, and **20c**). **Figure 19c** and **d** reveals that the density of low-angle boundaries was significantly reduced and grains with boundary angles higher than 15° were found in the microstructure. The microstructure in state S1

http://dx.doi.org/10.5772/intechopen.68954

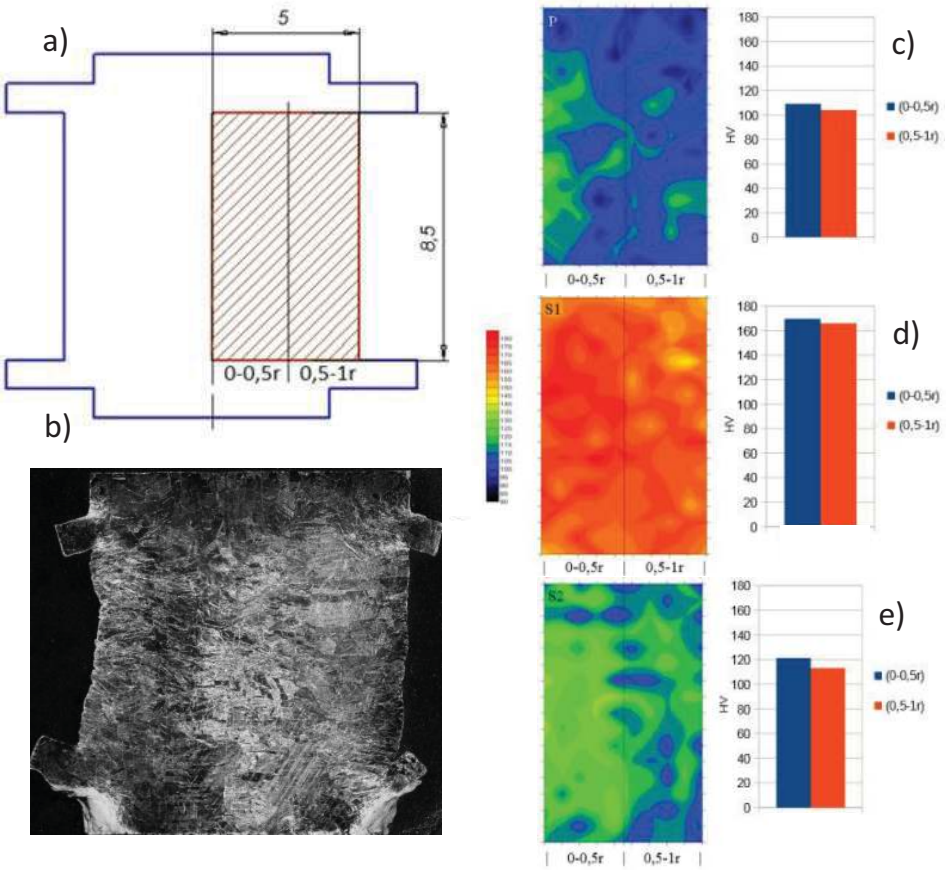

Figure 17. Distribution of measured hardness values on the longitudinal section (a, b) of CuCr0.6 samples after COT with parameters: torsion frequency $f = 0.8$ (Hz), compression rate $v = 0.015$ (mm/s), torsion angle $\alpha = \pm 6$ (°), and height reduction $h = 50$ (%). Total effective strain ($\varepsilon_f = 38$) for different initial structures; (c) P state; (d) S1 state; (e) S2.

is quite heterogeneous because a number of subgrains with low misorientation angles were observed in addition to the ultrafine grains with high misorientation angles (**Figure 20b**).

COT deformation with $\varepsilon_{ft} = 12$ typically exhibits the problem to eliminate the low-angle boundaries and transform the microstructure into one with higher angle boundaries (**Figure 21**).

The obtained results were confirmed by STEM investigations for $\varepsilon_{ft} = 28$and 45 (**Figure 22**). The COT process produces well-defined subgrain structures with low- and medium-angle misorientations that were identified based on the diffraction contrast (**Figure 22a**). With increasing strain, the structures observed in **Figure 22a** were comparable but additionally, a recovery process was observed in some microareas as shown in **Figure 22b**. This effect may be connected to the specifics of the deformation realized by the cyclic deformation. It is also possible

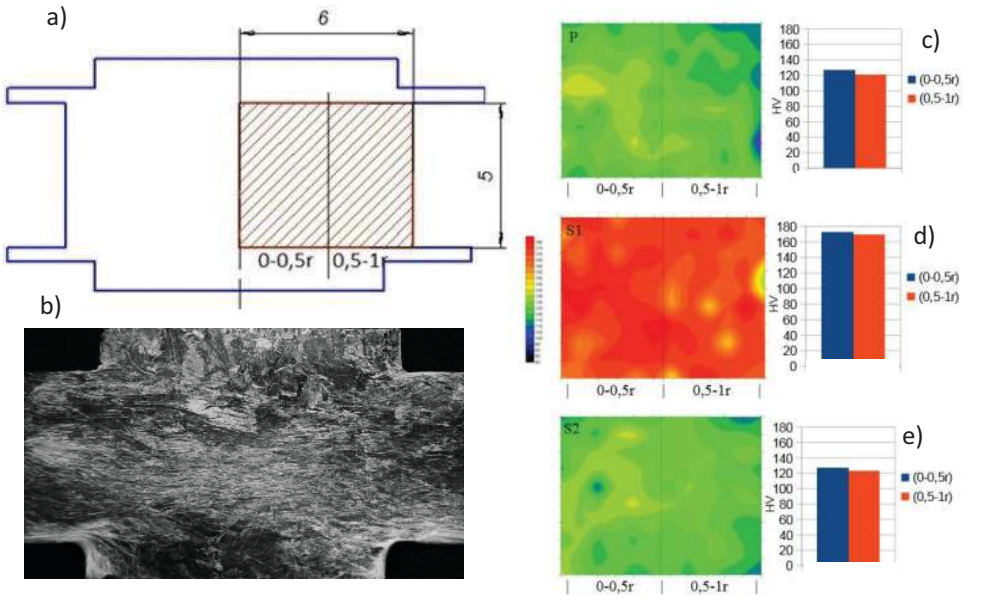

Figure 18. Distribution of measured hardness values on the longitudinal section (a, b) of CuCr0.6 samples after COT with parameters: torsion frequency f = 0.8 (Hz), compression rate v = 0.015 (mm/s), torsion angle α = ±6 (°), and height reduction h = 80 (%). Total effective strain (ε_f = 61) for different initial structures (c); P state; (d) S1 state; (e) S2 state.

that the temperature increased during the deformation and thus only an insignificant effect on the grain refinement is observed. The absence of small precipitates results in the effective loss of dislocations, which is unfavorable during the COT deformation. The lack of effective barriers for dislocation pinning gives rise to intensive recovery processes (**Figures 19a**, **b** and **22a**, **b**). For sample S1, the microshear banding contributes to the grain subdivision and the subgrain/grain structure dominates within the deformed bands (**Figure 22c**). Additionally, tangled dislocations are observed in the matrix. **Figure 22d** shows the microstructure of the CuCr0.6 alloy in the S1 state after the deformation at ε_{ft} = 45; it can be seen that the microstructure becomes more distinct and difficult to resolve. Many of the boundaries are not well-defined and are curved instead of straight, indicating the presence of a high internal stress. This type of microstructure is attributed to the development of arrays of high-energy non-equilibrium boundaries. Many dislocations are visible at both the grain boundaries and inside the grains. The typical microstructure for the S1 state becomes more heterogeneous than that of the P state (compare **Figures 22c**, **d** and **a**, **b**). With the increase of the deformation, the heterogeneity of the structure in the sample is still visible. This means that in this state, it is still more difficult for the high-energy boundaries to transform into stable arrays. We observe a very fine microstructure composed of grains that are smaller than 200 nm in sample S1. The microstructures of samples S2 processed for ε_{ft} = 28and ε_{ft} = 45 are shown in **Figures 22e** and **f**, respectively. The larger grains/subgrains coexist with small grains/subgrains. There are almost no dislocations in some grains/subgrains, and chaotically distributed dislocations

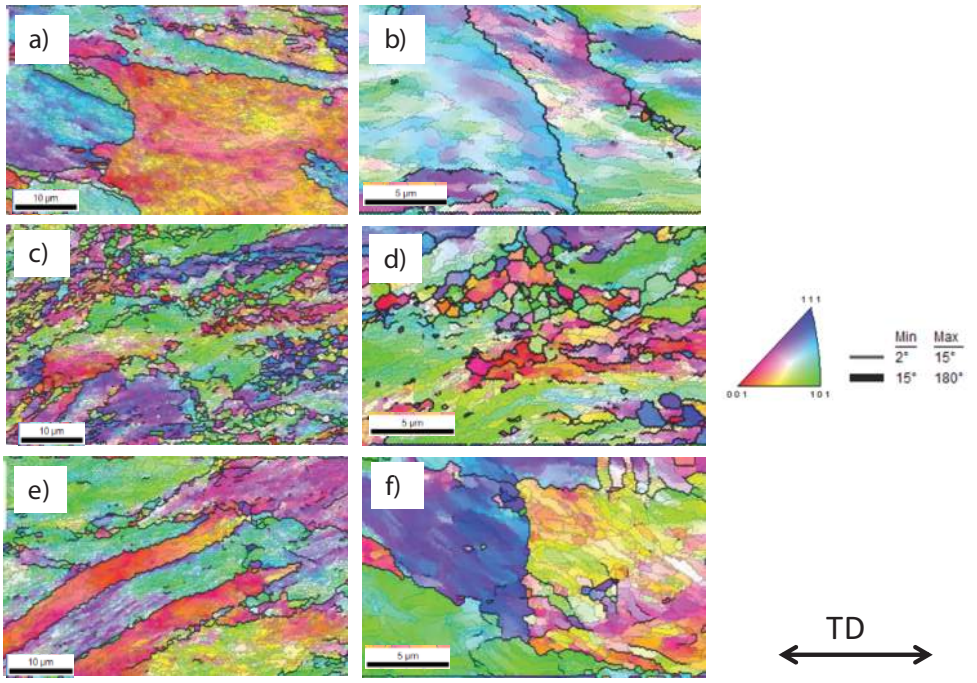

Figure 19. Orientation imaging maps ofCuCr0.6 sample showing deformed microstructures under different conditions: (a, b) P + COT state; (c, d) S1 + COT state; and (e, f) S2 + COT state. Deformation parameters: torsion frequency $f = 1.6$ (Hz), compression rate $v = 0.04$ (mm/s), torsion angle $\alpha = \pm 6$ (°), and height reduction $h = 80$ (%). Total effective strain ($\varepsilon_f = 45$).

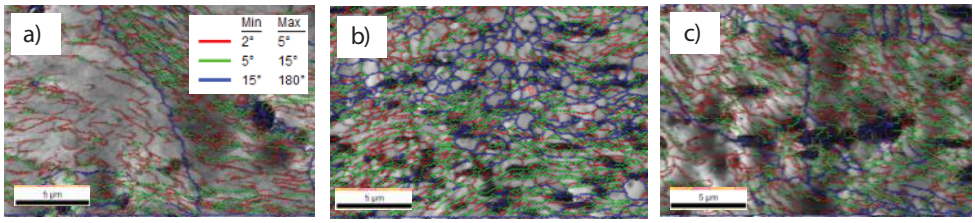

Figure 20. EBSD maps with different types of grain boundaries in CuCr alloys (a) P state, (b) S1 state, (c) S2 state. Deformation parameters: torsion frequency $f = 1.6$ (Hz), compression rate $v = 0.04$ (mm/s), torsion angle $\alpha = \pm 6$ (°), and height reduction $h = 80$ (%). Total effective strain ($\varepsilon_f = 45$).

are present in other large or small grains/subgrains. The average grain size was refined to about ~300–500 nm. From the literature [3–7], it is known that the microstructural evolution depends mainly on the strain magnitude, with a more homogeneous microstructure obtained with increasing strain. In our results, the differences in the microstructures are still observed even though the magnitude of the deformation increases. In general, it should be noted that it is impossible to obtain a homogeneous structure using this method.

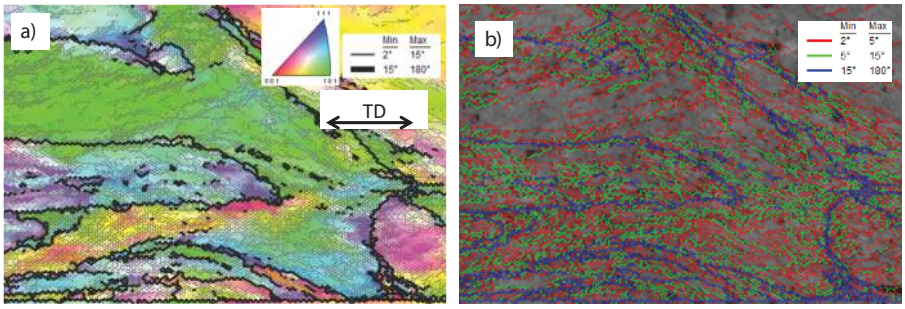

Figure 21. Orientation imaging map (a); and EBSD maps with different types of grain boundaries (b) for CuFe2 alloy after COT deformation with parameters: torsion frequency f = 1.6 (Hz), compression rate v = 0.1(mm/s), torsion angle α = ±6 (°), and height reduction h = 80 (%). Total effective strain (ε_f = 12).

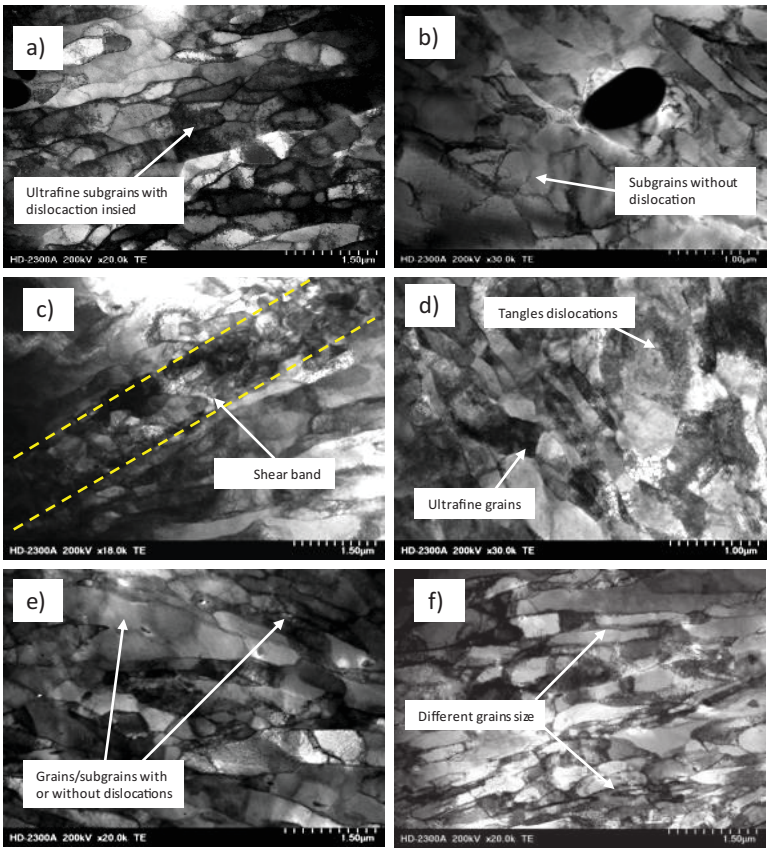

Figure_22.

Figure 22. STEM microstructures for CuCr0.6 alloy after COT deformation with parameters: (a) P state, ε_{ft} = 28, (b) P state, ε_{ft} = 45, (c) S1 state, ε_{ft} = 28, (d) S1 state, ε_{ft} = 45, (e) S1 state, ε_{ft} = 28, (f) S1 state, ε_{ft} = 45.

For the S1 state, COT processing hinders the deformation processes for both CuCr0.6 and CuFe2 alloys. For example, this can be clearly seen for $\varepsilon_{ft} = 28$ where coherent precipitates reduce the number of operating slip systems (**Figure 23a** and **b**). The much more equiaxed structures (S2 state) visible in **Figure 23c** and **d** are due to the occurrence of different slip systems.

The example distribution of the grain/subgrain diameter values for the CuCr0.6 alloy (P and S1 state) for $\varepsilon_{ft} = 45$ is shown in **Figure 24**.

It is important to note that based on SEM and STEM observations, the grain boundaries obtained during COT deformation are in the nonequilibrium state. It has been argued that such boundaries provide a large number of excess dislocations for the slip systems and can enable the grains to rotate at room temperature, leading to a significant increase in the strain hardening and ductility. The results of mechanical properties for CuCr0.6 and CuFe2 alloys are shown in **Figure 25** and in **Table 5**.

Several articles recently reported UFG materials maintaining both a high strength and an adequate ductility [6–9]. An especially high strength and good ductility in ultrafine-grained materials produced by the COT deformation were obtained for the S1 state. The fine precipitates interacted with the dislocations and exhibited a strong pinning effect on the dislocation movement, leading

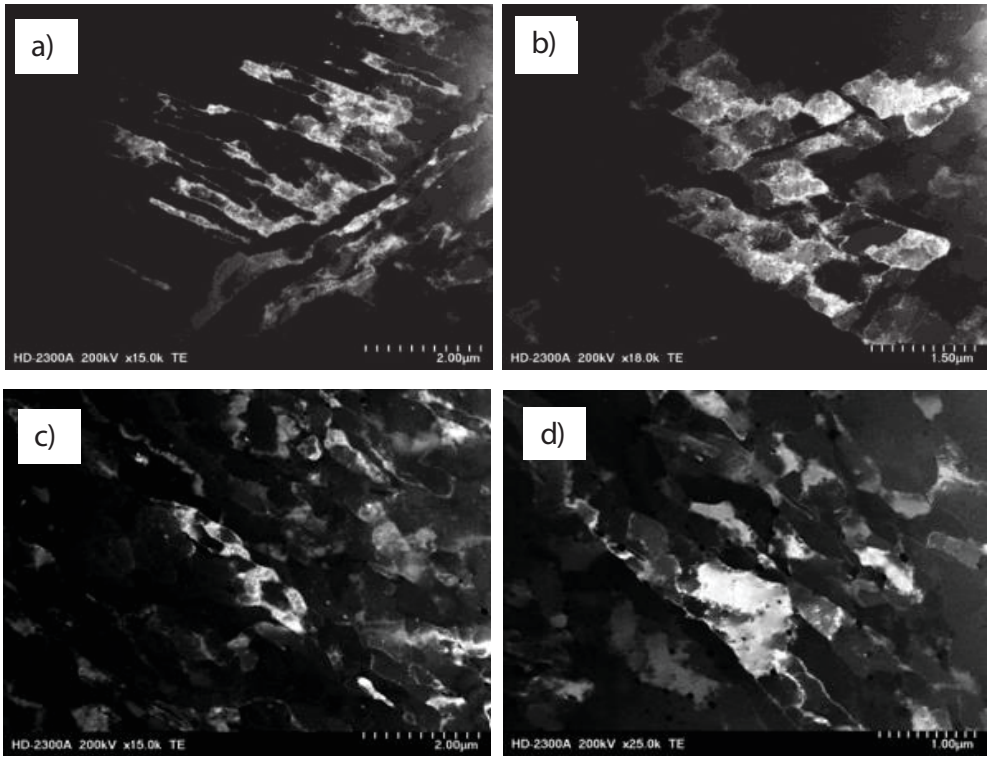

Figure 23. Dark field images obtained from STEM investigations for CuFe2 alloys after COT deformation with $\varepsilon_{ft} = 28$: (a, b) S1 state, (c, d) S2 state.

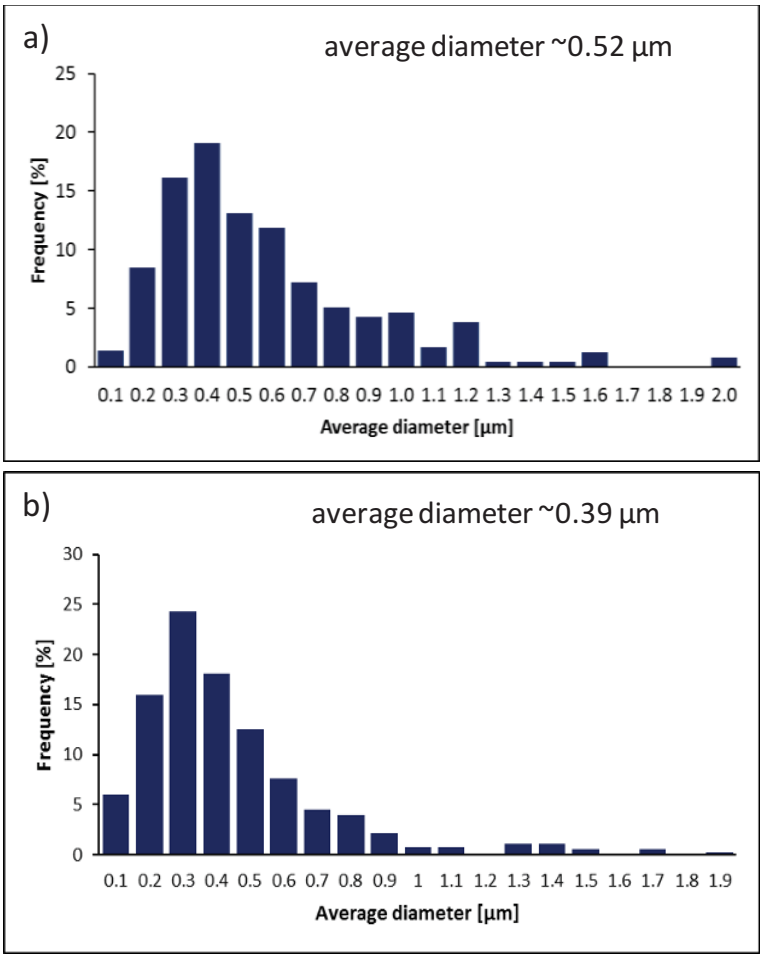

Figure 24. Grain/subgrain size distribution for CuCr0.6 alloy after COT deformation for $\varepsilon_{ft} = 45$: (a) P state, (b) S1 state.

to high yield strength (YS) and ultimate tensile strength (UTS) values. For the S2 state, the precipitates coarsened remarkably to an average size of 100 nm with a larger interparticle spacing. The coalescence of the precipitates accompanied by an enhanced recovery process resulted in a significant flow stress decrease. It is important to note that SPD processing leads to a reduction in the ductility that is generally smaller than those for the more conventional deformation processing techniques such as rolling, drawing, and extrusion. The low ductility is caused by the low strain-hardening rate, giving rise to early localized deformation in the form of necking. The availability of a bimodal (a mixture of two or multiphases with varying scales and properties) grain size distribution leads to a considerable increase in the ductility. We note that based on the obtained results, a significant degradation in the ductility of the specimens is typical for COT. The YS and UTS values are for the two alloys, comparable when are taken into account the heat

http://dx.doi.org/10.5772/intechopen.68954

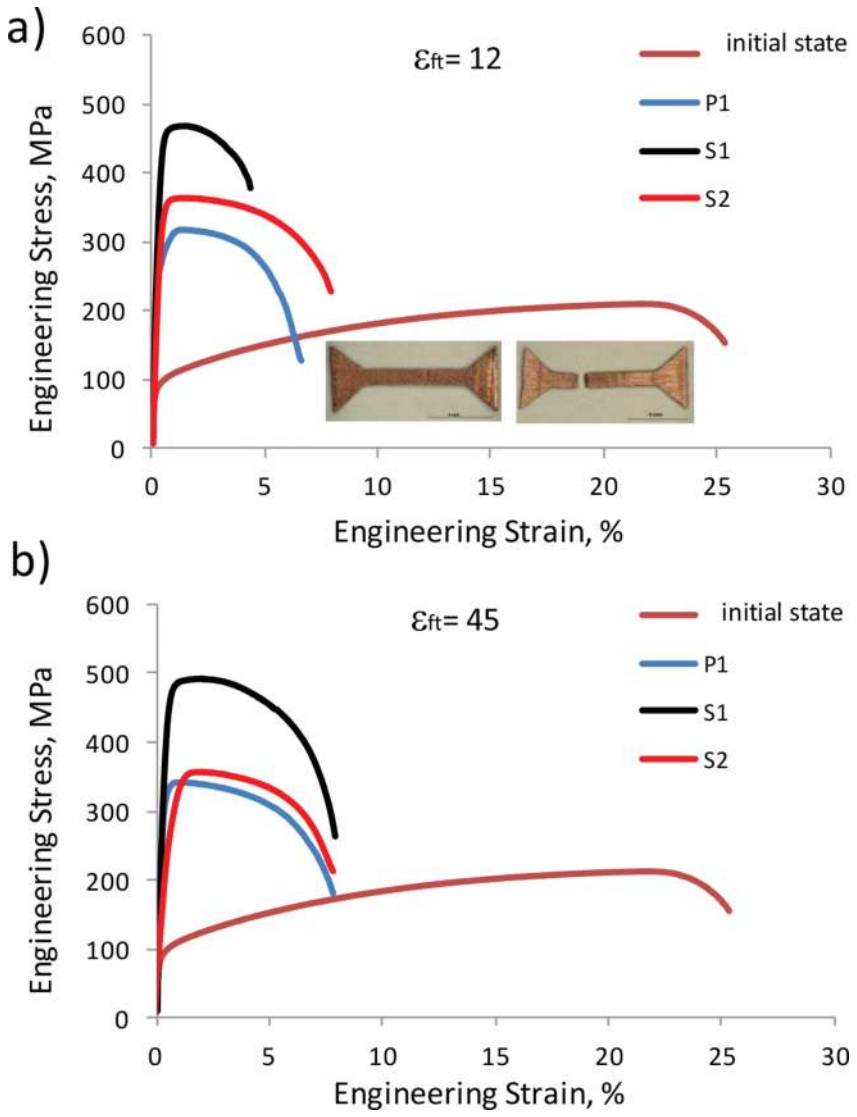

Figure 25. Engineering strain versus engineering stress for CuCr0.6 alloys after application of different magnitudes of total effective strain. a) e_{ft} = 12 and b) e_{ft} = 45.

treatment processes (maximal value of YS and UTS for S1 state), implying that a high content of Cr and Fe solute atoms in the Cu matrix of the deformed sample reduces the dislocation mobility and retards the dynamic recovery at a level comparable to that of the noncoherent but small particles observed for the S2 state. The pinning of the dislocation by these precipitates is much weaker but it does effectively influence the pinning of the grain/subgrain boundaries.

Material state		YS (MPa)	UTS (MPa)	A_{gt} (%)	A_c (%)	HV	IACS (%)
CuCr0.6	Initial state	97 ± 4	214 ± 5	22.5 ± 1	26.0 ± 1	43 ± 4	40
	Quenching + COT	336 ± 6	342 ± 6	1 ± 0.2	8 ± 0.8	123 ± 15	40
	Aging at 500°C/2 h + COT	464 ± 11	491 ± 3	1.8 ± 0.1	4.3 ± 0.3	180 ± 6.5	85
	Aging at 700°C/24 h + COT	343 ± 8	360 ± 7	1.7 ± 0.5	8.8 ± 1.5	132 ± 9	86
CuFe2	Initial state	148 ± 5	246 ± 4	14.2 ± 0.5	17.7 ± 0.6	60 ± 5	28
	Quenching + RCMR	329 ± 31	340 ± 34	1.8 ± 0.4	7.8 ± 1.6	126 ± 17	26
	Aging at 500°C/2 h + COT	378 ± 18	387 ± 17	1.6 ± 0.3	8 ± 1.4	150 ± 15	48
	Aging at 700°C/24 h + COT	309 ± 10	331 ± 17	2.6 ± 0.8	9.5 ± 1.8	133 ± 9	34

Table 5. Measured mechanical parameters: yield strength (YS), ultimate tensile strength (UTS), uniform elongation (A_{gt}), and elongation to fracture (A_c) of deformed CuCr0.6 and CuFe2 alloys using COT for $\varepsilon_{tt} = 45$.

6. Summary

The results obtained for the CuFe and CuCr alloys deformed through RCMR and COT indicated the possibility of obtaining materials with the UFG structure and high mechanical properties. During the RCMR and COT deformations, the microstructure was significantly refined but was heterogeneous after the application of a high total effective strain. Initially, the first process of deformation (lower value of total effective strain) dominates the development of deformation-induced boundaries that occur heterogeneously in the volume according to the net strain gradient. The measured grain/subgrain sizes are in the 200–500 nm range, with a mixture of low- and high-angle boundaries. In contrast to the commonly found statements in the literature, subsequent deformations (increased total effective strain) do not induce an increase of the grain misorientation and a decrease in the grain/subgrain size. Continuous heterogeneity in the microstructure increases in both alloys as a result of the cyclical character of these processes. Cyclic character of these methods promotes dynamic recovery, involving the decrease of dislocation density in the interior of grains/subgrains and in grain/subgrain boundaries.

The initial structure (heat treatment process) of the alloy influences the RCMR and COT deformations. The best combination of mechanical properties was obtained for the material deformed in the S1 state. The Fe and Cr precipitates in the S1 state that is responsible for the peak-aged strength of CuFe and CuCr alloys are expected to pin the dislocations. While the noncoherent particles in the S2 state are still capable of effectively pinning the grain

boundaries and prevent further coarsening, they are not as effective as the precipitates in the S1 state. The deformation sample in the P state shows hardening that is comparable to that of the S2 state and the deformation of the P samples results in a structure recovery.

The present investigation confirms that the cyclic deformation (RCMR and COT method) plays a significant role in the structure evolution. Especially, these processes decrease the rate of high angle boundaries (HABs) formation at the stages of large strain accumulation. Moreover, RCMR and COT deformations increase in the structure in homogeneity with increasing strain. Additionally, cyclic deformation processes did not affect, significantly, the effective grain refinement with increasing strain.

Acknowledgements

This work was supported by the National Science Centre in Poland under contract No. UMO-2013/09/B/ST8/01695.

Author details

Kinga Rodak

Address all correspondence to: kinga.rodak@polsl.pl

Faculty of Materials Engineering and Metallurgy, Silesian University of Technology, Katowice, Poland

References

[1] Prangnell PB, Bowen JR, Apps PJ. Ultra-fine grain structures in aluminium alloys by severe deformation processing. Materials Science and Engineering: A. 2004;**375-377**:178-185. DOI:10.1016/j.msea.2003.10.170

[2] Shaarbaf M, Toroghinejad MR. Nano-grained copper strip produced by accumulative roll bonding process. Materials Science and Engineering: A. 2008;**473**:28-33. DOI: 10.1016/j.msea.2007.03.065

[3] Chinh NQ, Horvath G, Horita Z, Langdon TG. A new constitutive relationship for the homogeneous deformation of metals over a wide range of strain. Acta Materialia. 2004;**52**:3555-3563. DOI: 10.1016/j.actamat.2004.04.009

[4] Aldazabal J, Sevillano JG. Hall-Pech behaviour induced by plastic strain gradiens. Materials Science and Engineering: A. 2004;**365**:186-190. DOI: 10.1016/j.msea.2003.09.026

[5] Mishra A, Kad BK, Gregori F, Meyers MA. Microstructural evolution in copper subjected to severe plastic deformation: Experiments and analysis. Acta Materialia. 2007;**55**:13-28. DOI: 10.1016/j.actamat.2006.07.008

[6] Orlov D, Beygelzimer Y, Synkov S, Varyukhin V, Tsuji N, Horita Z. Microstructure evolution in pure Al processed with twist extrusion. Materials Transactions. 2009;**50**:96-100. DOI: 10.2320/matertrans.MD200802

[7] Huang WH, Yu CY, Kao PW, Chang CP. The effect of strain path and temperature on the microstructure developed in copper processed by ECAE. Materials Science and Engineering: A. 2004;**366**:221-228. DOI: 10.1016/j.msea.2003.08.033

[8] Dobatkin SV, Szpunar JA, Zhilyaev AP, Cho JY, Kuznetsov AA. Effect of the route and strain of equal-channel angulat pressing on structure and properties of oxygen-free copper. Materials Science and Engineering: A. 2007;**462**:132-138. DOI: 10.1016/j.msea.2006.04.156

[9] Sun PL, Yu CY, Kao PW, Chang CP. Microstructural characteristics of ultrafine-grained aluminium produced by equal channel angular extrusion. Scripta Materialia. 2002;**47**:377-381. PII: S1359-6462(02)00117-3

[10] Ferry M, Burhan N. Structural and kinetic aspect of continuous grain coarsening in a fine-grained Al-0.3Sc alloy. Acta Materialia. 2007;**55**:3479-3491. DOI: 10.1016/j.actamat.2007.01.047

[11] Apps PJ, Berta M, Prangnell PB. The Effect of dispersoids on the grain refinement mechanisms during deformation of aluminium alloys to ultra-high strains. Acta Materialia. 2005;**53**:499-511. DOI: 10.016/j.actamat.2004.09.042

[12] Valipour Sh, Eivani AR, Jafarian HR, Seyedein SH, Aboutalebi MR. Effect of pre-deformation termomechanical processing on the development of ultrafine grain structure during equal channel angular extrusion. Materials & Design. 2016;**89**:377-384. DOI: 10.1016/j.matdes.2015.09.161

[13] Quadir MZ, Ferry M, Al-Buhamad O, Munroe PR. Shear banding and recrystallization texture development in a multilayered Al alloy sheet produced by accumulative roll bonding. Materials & Design. 2009;**57**:29-40. DOI: 10.1016/j.actamat.2008.08.056

[14] Rodak K, Radwański K. Influence of precipitates on the grain refinement in CuFe2 alloy processed by rolling with cyclic movement of rolls. Materials and Design. 2016;**110**:255-265. DOI: 10.1016/j.matdes.2016.07.138

[15] Rodak K, Pawlicki J. Microstructure characterization of Cu processed by compression with oscillatory torsion. Materials Characterization. 2014;**94**:37-45. DOI. 10.1016/j.matchar.2014.05.002

[16] Rodak K, Pawlicki J.Effect of compression with oscillatory torsion processing on structure and properties of Cu. Journal of Materials Science & Technology. 2011;**27**:1083-1088. http://www.jmst.org/EN/Y2011/V27/I11/1083

[17] Rodak K, Pawlicki J. Efficiency of the compression with oscillatory torsion method in grain refinement in Al. Archives of Civil and Mechanical Engineering. 2016;**16**:805-812. DOI. 10.1016/j.acme.2016.05.004

[18] Rodak K, Radwański K, Molak R, Pakiela Z. Studies of Cu after plastic deformation. Kovove Materialy Metalic Materials. 2010;**48**:313-319. DOI: 10.4149/km_2010_5_313

[19] Rodak K, Molak RM, Pakieła Z. Structure and properties of copper after large strain deformation. Physica Status Solidi (C). 2010;**5**:1351-1354. DOI: 10.1002/pssc.200983392

[20] Dobatkin SV, Gubicza J, Shangina DV, Bochvar NR, Tabachkova NY. High strength and good electrical conductivity in Cu-Cr alloys processed by severe plastic deformation. Materials Letters. 2015;**153**:5-9. DOI: 10.1016/j.matlet.2015.03.144

[21] Vinogradov A, Ishida T, Kitagawa K, Kopylov VI. Effect of strain path on structure and mechanical behaviour of ultra-fine grain Cu-Cr alloy produced by equal-channel angular pressing. Acta Materialia. 2005;**53**:2181-2192. DOI:10.1016/j.actamat.2005.01.046

[22] Islamgaliev RK, Nesterov KM, Bourgon J, Champion Y, Valiev RZ. Nanostructured Cu-Cr alloys with high strength and electrical conductivity. Journal of Applied Physics. 2014;**115**:194301-194304. DOI: 10.1063/1.4874655

[23] Wei KX, Wei W, Wang F, Du QB, Alexandrov IV, Hu J. Microstructure, mechanical properties and electrical conductivity of industrial Cu-0.5%Cr alloy processed by severe platic deformation. Materials Science and Engineering: A. 2011;**528**:1478-1484. DOI:10.1016/j.msea.2010.10.059

[24] Cao H, Min JY, Wu SD, Xian AP, Shang JK. Pinning of grain boundaries by second phase particles in equal-channel angularly pressed Cu_Fe_P alloy. Materials Science and Engineering: A. 2006;**431**:86-91. DOI: 10.1016/j.msea.2006.05.081